Polarization effect on He doubly excited states below the $N=2$ threshold of He^+

Jun Yan,[1] Yi-Zhi Qu,[1] Lan Voky,[2] and Jia-Ming Li[1,3]
[1]*Institute of Physics, Chinese Academy of Science, Beijing 100080, China*
[2]*Nice Observatoire, URA 1362 du CNRSBP 226, O6304 Nice, France*
[3]*Center of Atomic and Molecular Sciences, Department of Physics, Tsinghua University, Beijing 100084, China*
(Received 29 April 1997; revised manuscript received 4 September 1997)

Based on the R-matrix method, photoionization cross sections of He below the $N=2$ threshold of He^+ are calculated, and a definite assignment of the doubly excited resonance states is determined by the eigenchannel treatment. Our results are in good agreement with the experimental data and other theoretical works. The polarization effects on the doubly excited states are studied in detail. We elucidate the effects of the dynamic polarization within the reaction zone (i.e., R-matrix box) and the long-range static polarization potentials outside the reaction zone, which influence the resonance energies and the profiles of He resonance states. [S1050-2947(98)00802-6]

PACS number(s): 32.80.Fb, 32.80.Dz, 32.70.−n

I. INTRODUCTION

Helium is the simplest prototype neutral atomic system that exhibits strong electron-electron correlation. After the first observation of doubly excited states of He by Madden and Codling [1], and the theoretical explanation by Fano, Copper, and Prats [2–4], many experimental [5–9] as well as theoretical [10–33] efforts have been focused on the photoionization spectrum of He. In recent years, with an energy resolution of $\cong 4$ meV, Domke and co-workers [7,8] have observed all three autoionization resonance series, i.e., $(sp,2n^+)^1P^o$, $(sp,2n^-)^1P^o$ and $(2pnd)^1P^o$ series of He below the $N=2$ threshold of He^+ in a photoionization experiment using synchrotron radiation. They gave an empirical assignment for $(sp,2n^-)$ and $(2pnd)$ states. Some resonance energies of the $(sp,2n^-)$ and $(2pnd)$ states were also given by fitting the measured photoionization spectra to a standard Fano profile for the $(sp,2n^-)$ lines and near-symmetric monochromator function corresponding to a weighted sum of Gaussian and Lorentzian profiles for the $(2pnd)$ lines. Schulz *et al.* [9] remeasured these three series with an improvement in spectral resolution of 1 meV. Their observation of the very narrow $(2pnd)$ and $(sp,2n^-)$ series established a firm basis for testing the accuracy of theoretical calculations.

Theoretically, the $(sp,2n^{\pm})$ and $(2pnd)$ doubly excited series of He have been studied extensively in the past decades. Various theoretical works have been reported, including configuration-interaction (CI) methods [10–13], hyperspherical coordinate methods [14–16], close-coupling approximations [17–19], R-matrix methods [20–23], Feshbach projection formalism [24–30], and others such as the complex-coordinate rotation method [31,32]. For the $(sp,2n^{\pm})$ states, almost all the theoretical methods produced similar results in terms of Fano parameters (the resonance energy E_r, width Γ, and q parameter). For the extremely narrow $(2pnd)$ series, it is a much stringent test for numerical calculations. Before the observation in Ref. [7], some theoretical calculations [11,19,27,29–32] gave the resonance energies in a correct order $[E_r(2pnd)<E_r(sp,2(n+1)^-)]$, and some theoretical calculations [17,21,22,24], including the early R-matrix calculations [21,22], gave the incorrect order $[E_r(sp,2(n+1)^-)<E_r(2pnd)]$. After the observation Ref. [7], there followed Chang's calculation [12] using the CI method, and Tang, Watanabe, and Matsuzawa's calculation [16] using the hyperspherical close-coupling method. Both focused their attention mainly on the extremely narrow $(2pnd)$ states. Their results were in agreement with experimental results [7].

In the present paper, we employ the R-matrix method [34–38] to calculate the photoionization cross sections of He below the $N=2$ threshold of He^+ in order to provide a test of the accuracy of the R-matrix method. Using the eigenchannel treatment of R-matrix theory [39,40], we can give a definite assignment for all resonance states. Our theoretical results, i.e., the photoionization cross sections and the Fano parameters, are in general agreement with the experimental results [7] and other theoretical results. For the extremely narrow $(2p3d)$ state, our calculated spectra are in better agreement with the experimental results [7] than the recent theoretical works [12,16]. Furthermore, we elucidate the effects of the dynamic polarizations within the reaction zone (i.e., R-matrix box) and the long-range static polarization potentials outside the reaction zone, which influence the resonance energies and the profiles of the resonance states. Here the dynamic polarizations are defined as interactions (with exchange-type interactions) involving the transform of parity and angular momenta between the scattered electron and the target electrons. The physical mechanism of the energy redshift for $(sp,2n^-)$ resonances and the energy blueshift for $(sp,2n^+)$ resonances is discussed. In the R-matrix calculation which treat the bound states and continuum states on the same footing, we also present the ionization energy for the He ground state $(1s^2)^1S$ and the quantum defects for He excited states. Through analyses of quantum defects for the excited states, one should adopt Herzberg's ionization energy $198\,310.8\pm0.15$ cm^{-1} [41] instead of the Moore's value $198\,310\pm15$ cm^{-1} [42].

II. THEORY AND RESULTS

Detailed descriptions of R-matrix theory were given in Refs. [34–38]. In R-matrix theory, a value a of the radial

TABLE I. The percentage of static polarizability $P\%$ with respect to $1s$, $2s$, and $2p$ of He^+, and the R-matrix box radius a for each target set.

Target set	1	2	3	4
$P\%$ to $1s$	75	78	79	100
$P\%$ to $2s$	75	85	88	89
$P\%$ to $2p$	83	91	94	100
a	19.8	30.6	43.4	21.6

variable r is chosen such that the exchange interactions between the scattered electron and the target electrons is negligible for $r \geqslant a$, where a is the R-matrix box radius. Within the reaction zone ($r \leqslant a$), the interactions between the scattered electron and target electrons involve static electron-electron screening, dynamic polarizations, etc. It is a many-body problem, which is solved variationally as a whole system to obtain the logarithmic derivative boundary matrix $\mathcal{R}(E)$.

Outside the reaction zone, the scattered electron ''feels'' mainly Coulomb potential. The updated R-matrix code [37,38] allows us to take the long-range static polarization potentials into account. The wave function of the scattered electron outside the reaction zone satisfies the radial equation (in atomic units, with energy in Rydberg throughout the paper if not specified),

$$\left(\frac{d^2}{dr^2}-\frac{l_i(l_i+1)}{r^2}+\frac{2z}{r}+\varepsilon_i\right)F_i(r)-\sum_{i'}^{n} V_{ii'}(r)F_{i'}(r) = 0 \quad i=1,\ldots,n, \tag{1}$$

where n is the number of coupled channels, and $V_{ii'}(i \neq i')$ are long-range multipole potentials,

$$V_{ii'}(r)=\sum_{\lambda} C_{ii'}^{(\lambda)}/r^{\lambda+1}. \tag{2}$$

In practice, only contributions of $\lambda=1$ and 2, which correspond to the dipole and quadrupole polarization potentials, are included. Because $|V_{ii'}(r)| \ll 2z/r$ for $r \geqslant a$, the multipole potentials are therefore treated as perturbations [37].

Matching the logarithmic derivative boundary matrix $\mathcal{R}(E)$ on the R-matrix box surface (i.e., $r=a$), the wave function $F_{ii'}$ outside the reaction zone is solved numerically. Depending on the energy range of interest, $F_{ii'}$ should have the following well-known asymptotic boundary conditions at infinity [34] respectively: (1) the standard scattering asymptotic boundary condition with the reactance matrix in the energy range with all open channels; (2) the standard bound-state asymptotic boundary condition with exponentially decaying radial wave functions in the energy range of all closed channels; and (3) in the autoionization energy range, the standard scattering asymptotic boundary condition with the reactance matrix for i belonging to the open channels, and the asymptotic boundary condition with the exponentially decaying radial wave functions for i belonging to the closed channels. Thus the physical solutions of the initial and final states can be obtained with the boundary conditions at $r=a$ and at infinity. The photoionization cross sections are obtained by integrating the dipole operator (either the length or the velocity operator) between the initial and final states.

To elucidate the polarization effects in the He photoionization process, we use the following four sets of target functions:

target set 1: $1s,2s,2p,3s,3p,3d$,

target set 2: $1s,2s,2p,3s,3p,3d,4s,4p,4d,4f$,

target set 3: $1s,2s,2p,3s,3p,3d,4s,4p,4d,5s,5p,5d,5f,5g$,

target set 4: $1s,2s,2p,3s,3p,3d,\overline{4s},\overline{4p},\overline{4d}$,

where $1s$–$5g$ are hydrogenlike wave functions of He^+. $\overline{4s}$, $\overline{4p}$, and $\overline{4d}$ are polarized orbitals of He^+ calculated using the CIVPOL code [43]. For each target set, the static polarizability considered with respect to $1s$, $2s$, and $2p$ of He^+ and the R-matrix box radius are given in Table I. When one carries out the R-matrix calculations, the degree of the dynamic polarizations included within the reaction zone should be consistent with the static polarizabilities in Table I. Outside the reaction zone, $F_{ii'}$ can be obtained either with or without $V_{ii'}$. Therefore we can analyze the effects of the dynamic polarizations within the reaction zone and the static polarization potentials outside the reaction zone in the He photoionization process.

The wave functions of the initial ground state $(1s^2)^1S$ and final continuum states are obtained on the same footing. The ground state has an energy of $E=-4-I$ obtained through the variational principle, where I is the ionization energy. Table II gives values of I calculated using the above four target sets with $V_{ii'} \neq 0$. The ionization energy I converges to the nonrelativistic limit 1.8074 Ry [44] from target set 1 to target set 4. The dynamic polarizations considered within the

TABLE II. Ionization energies I for the He ground state $(1s^2)^1S$.

States included in expansion	I	Reference
$1s$	-1.7450	Ref. [45]
$1s,\overline{2p},\overline{3d}$	-1.7817	Ref. [45]
$1s,2s',\overline{2p},2p',\overline{3d}$	-1.8007	Ref. [45][a]
$1s,2s,2p,\overline{3p},\overline{3d}$	-1.7868	Ref. [21][b]
Target set 1, 2, 3, 4	-1.7732, -1.7741, -1.7742, -1.7908	present work
Pekeris's result	-1.8074	Ref. [44]

[a]With short-range correlation orbitals $2s',2p'$.

[b]Previous R-matrix calculation.

TABLE III. Quantum defects μ for He-excited states.

States	Theory		Expt.	
	target set 1	target set 4	a	b
$1s2s\ ^1S$	0.140	0.145	0.149	0.149
$3\ ^1S$	0.133	0.139	0.143	0.144
$4\ ^1S$	0.131	0.137	0.141	0.143
$5\ ^1S$	0.131	0.136	0.141	0.144
$6\ ^1S$	0.130	0.136	0.140	0.146
$1s2s\ ^3S$	0.310	0.311	0.311	0.311
$3\ ^3S$	0.302	0.302	0.302	0.303
$4\ ^3S$	0.299	0.299	0.299	0.301
$5\ ^3S$	0.298	0.298	0.298	0.301
$6\ ^3S$	0.297	0.298	0.297	0.303
$1s2p\ ^1P^o$	−0.0126	−0.0105	−0.0095	−0.0091
$3\ ^1P^o$	−0.0150	−0.0125	−0.0113	−0.0104
$4\ ^1P^o$	−0.0156	−0.0130	−0.0119	−0.0099
$5\ ^1P^o$	−0.0159	−0.0132	−0.0121	−0.0085
$6\ ^1P^o$	−0.0160	−0.0133	−0.0123	−0.0061
$1s2p\ ^3P^o$	0.0592	0.0615	0.0622	0.0625
$3\ ^3P^o$	0.0624	0.0651	0.0658	0.0667
$4\ ^3P^o$	0.0634	0.0662	0.0668	0.0687
$5\ ^3P^o$	0.0639	0.0667	0.0672	0.0707
$6\ ^3P^o$	0.0641	0.0670	0.0673	0.0732
$1s3d\ ^1D$	0.001 43	0.001 88	0.001 57	0.002 48
$4\ ^1D$	0.001 52	0.001 86	0.001 66	0.003 63
$5\ ^1D$	0.001 57	0.001 90	0.001 69	0.005 33
$6\ ^1D$	0.001 59	0.001 93	0.001 69	0.007 80
$1s3d\ ^3D$	0.001 85	0.002 31	0.001 97	0.002 89
$4\ ^3D$	0.002 10	0.002 46	0.002 21	0.004 17
$5\ ^3D$	0.002 23	0.002 58	0.002 29	0.005 93
$6\ ^3D$	0.002 30	0.002 65	0.002 33	0.008 44

reaction zone increase a little from target set 1 to target set 3, as shown in Table I; consequently the value of I only increase a little (from 1.7732 to 1.7742 Ry). For target set 4, the percentage of static polarizability for $1s$ of He^+ increase to 100% by including the polarized orbitals, and a significant improvement of I is obtained (from 1.7742 to 1.7908 Ry). In order to obtain better ground-state energy, it is necessary to take the short-range correlations into account further [45].

On the same footing, we also calculate excited-state energies of $E=-4-4/(n-\mu)^2$, where μ is the quantum defect. Table III gives the μ for He excited states $(1sns)^{1,3}S$, $(1snp)^{1,3}P$, and $(1snd)^{1,3}D$ calculated based on target sets 1 and 4. For the penetrating Rydberg series $(1sns)^{1,3}S$ and $(1snp)^{1,3}P$, the μ of target set 4 agree better with the experimental results [42,41] than those of target set 1. For the nonpenetrating Rydberg series of $(1snd)^{1,3}D$, the μ's calculated based on target set 4 are greater than the experimental results (column a) of Moore [42] with $1R_\infty = 109\,737.32\ \mathrm{cm}^{-1}$ (without taking into account the reduced mass of the electron). Since the excited-state energies are obtained through the variational principle, they should not be deeper than the experimental energy levels, i.e., μ's should be smaller than the experimental results. Here we notice that for $(1snd)^{1,3}D$ states, the μ's are very small $(\sim 10^{-3})$, and the effect of reduced mass of the electron is just about the same order. Therefore the Rydberg constant $1R_M = 109\,722.27\ \mathrm{cm}^{-1}$ of He should be used to convert energy levels to a quantum defects. Even if R_M is used, the quantum defects (target set 4) of $1s3d^{1,3}D$ are still greater than the experimental values calculated using the ionization threshold $I = 198\,305 \pm 15\ \mathrm{cm}^{-1}$ of Moore [42]. The experimental μ's in the last column b of Table III, which are calculated with the ionization threshold $I = 198310.8 \pm 0.15\ \mathrm{cm}^{-1}$ of Herzberg [41], are all greater than our theoretical results. This is consistent with the variational principle. After taking into account the relativistic corrections and QED corrections, Pekeris's nonrelativistic limit I [44] is in excellent agreement with Herzberg's value I.

The scattered electron wave functions can be obtained by either with or without $V_{ii'}$. When $V_{ii'}=0$, we can easily perform an eigenchannel treatment of R-matrix theory [39,40]. We start with the logarithmic derivative boundary matrix $\mathcal{R}(E)$, and the physical eigenchannel parameters (eigen quantum defects μ_α and orthogonal transformation matrix $U_{i\alpha}$) in multichannel quantum defect theory (MQDT) [47–55], and the corresponding eigenchannel wave functions are calculated directly. Based on the compact set of the eigenchannel parameters, atomic perturbed discrete Rydberg series, autoionizing states and their adjacent continuum can be treated in an analytical unified manner without any numerical integrations outside the R-matrix box. In the analytical unified treatment of MQDT, we can offer a clear assignment for all resonances. The detailed description of the eigenchannel treatment of R-matrix theory will be given in the Appendix.

Figure 1 displays the calculated photoionization cross section for $(2p3d)$ and $(sp,24^-)$ states. The spectra in Figs. 1(a)–1(d) are calculated with $V_{ii'}=0$ using target sets 1–4 respectively. The spectra in Figs. 1(a′)–1(d′) are calculated with $V_{ii'}\neq 0$. In Figs. 1(a) and 1(a′), the profiles of length formula and velocity formula for $(2p3d)$ are quite different. This suggests that the calculated results of the doubly excited resonance $(2p3d)$ have not converged for target set 1. In Figs. 1(b) and 1(b′), the profiles of length formula and velocity formula for $(2p3d)$ are similar. This means the results of target set 2 are going to converge. In Figs. 1(c) and 1(d) and 1(c′) and 1(d′), the profiles converge much better quantitatively. Notice that the static polarizabilities increase by an appreciable amount from target set 1 to target set 2 (more specifically, from 75% to 85% for $2s$, and from 83% to 91% for $2p$) as shown in Table I. This suggests that the convergence of the $(2p3d)$ profile results from the increasing degree of the dynamic polarizations considered within the reaction zone.

By comparing Figs. 1(d) and 1(d′), one can elucidate the effect of the static polarization potentials outside the reaction zone. After taking into account the static polarization poten-

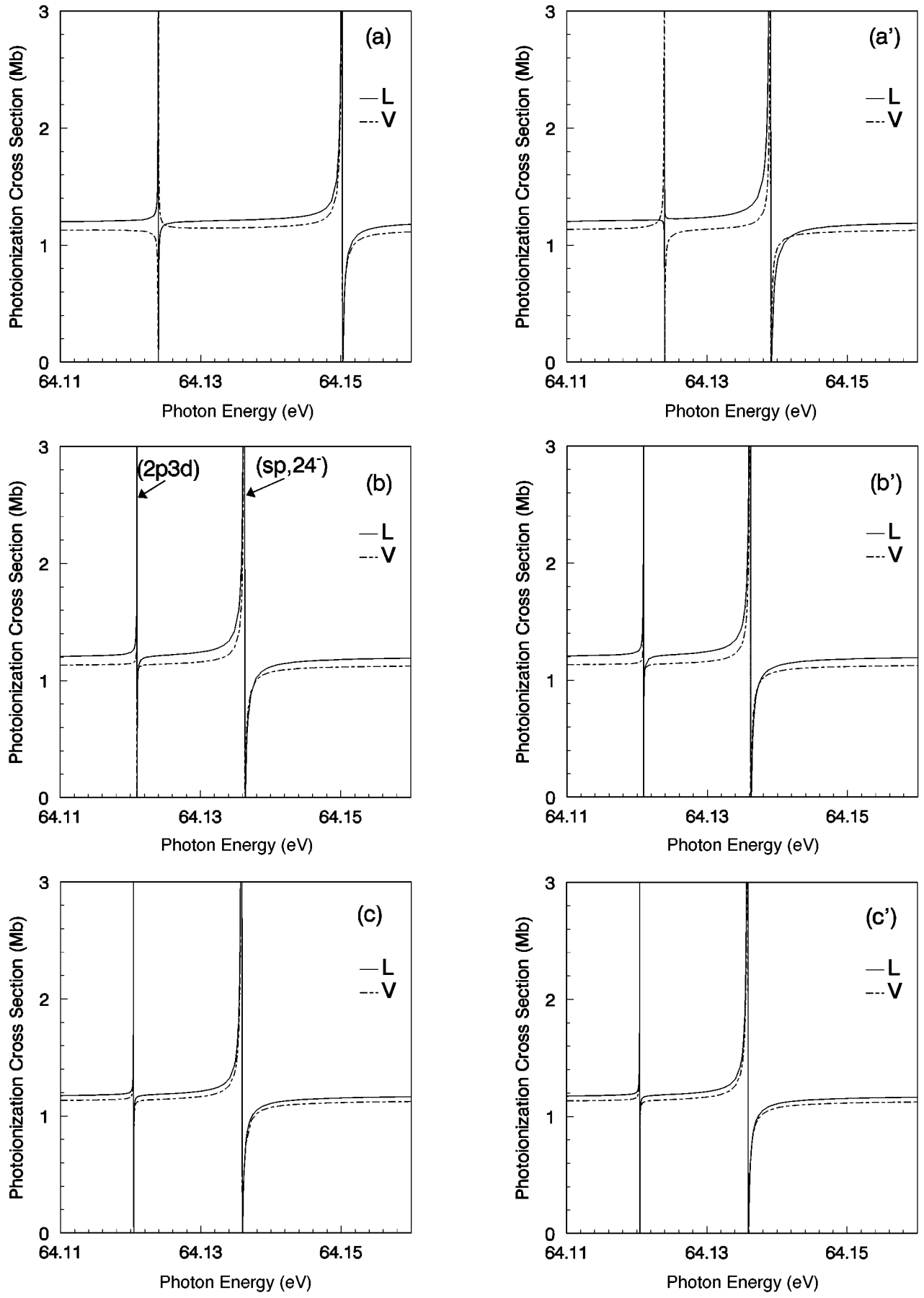

FIG. 1. The photoionization spectra for $(2p3d)$ and $(sp,24^-)$ resonance states. (a)–(d) correspond to target set 1–4 with $V_{ii'}=0$. (a′)–(d′) correspond to target set 1–4 with $V_{ii'}\neq 0$.

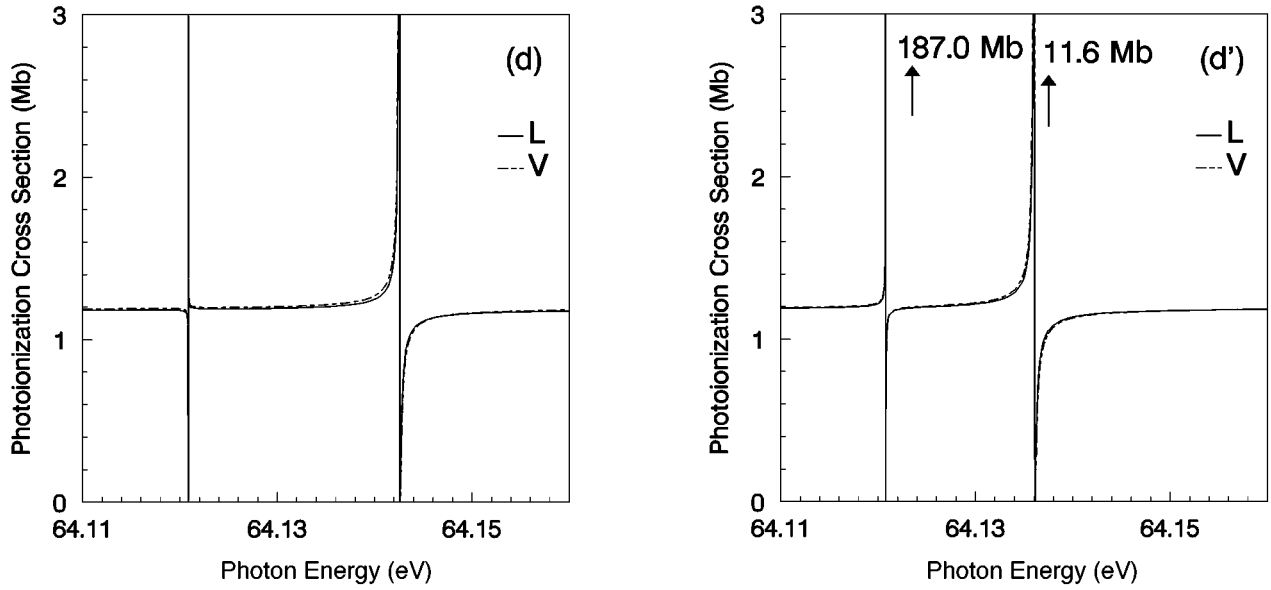

FIG. 1. (*Continued*).

tials outside the reaction zone, the profile changes and the resonance position almost does not change for $(2p3d)$ resonance states, while, for the $(sp,24^-)$ resonance state, the profile does not change and the resonance position moves deeper. Figure 2 displays the calculated photoionization cross section for the $(sp,24^+)$ state using target set 4. After taking into account the static polarization potentials outside the reaction zone, the profile for the $(sp,24^+)$ state does not change, and its resonance position moves higher. There is little difference between the spectra in Figs. 1(b) and 1(b′). Therefore we can easily perform the eigenchannel treatment of R-matrix theory, and call the left resonance peak a $(2p3d)$ state and the right one a $(sp,24^-)$ peak. Our calculation shows that peak photoionization cross sections $\sigma_{\max}$ of a $(2pnd)$ series are much greater than those of a $(sp,2n^-)$ series, as shown in Fig. 1(d′).

III. DISCUSSION

In the R-matrix calculation, the wave functions of the initial ground state, excited states, and final continuum states

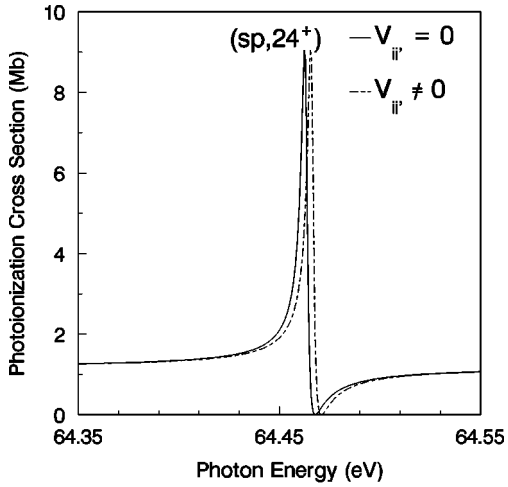

FIG. 2. The photoionization spectrum for the $(sp,24^+)$ resonance state calculated.

are calculated on the same footing. For target set 4, the static polarizability for $He^+(1s)$ is 100% as shown in Table I; consequently the dynamic polarizations are taken into account sufficiently within the reaction zone. Therefore the ionization energy of target set 4 in Table II agrees with Pekeris's nonrelativistic limit [44] within 1%. For the penetrating Rydberg series $^{1,3}S$ and $^{1,3}P$, the quantum defects of target set 4 are also in good agreement with experimental results as shown in Table III. For the nonpenetrating Rydberg series of $(1snd)^{1,3}D$, the quantum defects are very small ($\sim 10^{-3}$), and the effect of reduced mass of the electron is just about the same order. Therefore we should use a Rydberg constant corresponding to the reduced mass of the electron. Since the theoretical quantum defects obtained by the variational principle should not be greater than the experimental values, and the quantum defects are sensitive to the adopted experimental ionization threshold, one should adopt Herzberg's value 198 310.8 ± 0.15 cm^{-1} [41] instead of Moore's value 198 310 ± 15 cm^{-1} [42] through the analyses of quantum defects.

With the increasing degree of the dynamic polarizations considered within the reaction zone (i.e., from target set 1 to target set 4), the calculated photoionization cross sections converge, as shown in Fig. 1. For target set 4, whose R-matrix radius is 21.6 a.u., the spectra for $(2p3d)$ and $(sp,24^-)$ states calculated with and without $V_{ii'}$ are quite different as shown in Figs. 1(d) and 1(d′); for target set 2, whose R-matrix radius is 30.6 a.u., the spectra are similar, as shown in Figs. 1(b) and 1(b′). This suggests that the long-range static polarization potentials, which have influence on the spectra for $(2p3d)$ and $(sp,24^-)$ resonance states, are important in the range of $r = 20$–30 a.u. When the R-matrix box is large, as in the case of target set 2, we can make a definite assignment for all resonance states using the eigenchannel treatment of R-matrix theory [39,40], without $V_{ii'}$. $V_{ii'}$ are attractive for the $(sp,2n^-)$ state, and exclusive for the $(sp,2n^+)$ state, as shown in Figs. 1(d), 1(d′), and 2. This can be understood as follows: for $(sp,2n^-)$ states, the scattered electron will face the positive end of the electric dipole

TABLE IV. Resonance energies E_r, widths Γ, and the line-shape parameters q for doubly excited $^1P^o$ states of He below the $N=2$ threshold. The number $a[b]$ denotes $a\times10^b$. The numbers in parentheses for experimental data represent the error bars in units of the last digit.

State	Observed			Theory					
	Ref. [6]	Refs. [7,8]	Ref. [9]	Present	Ref. [19]	Ref. [32]	Ref. [16]	Ref. [12]	Ref. [21]
				Resonance energy E_r (eV)					
2+	60.151(10)	60.147	60.1503(40)	60.160	60.184	60.145	60.156	60.147	60.189
3+	63.655(10)	63.658	63.6575(30)	63.659	63.670	63.656	63.658	63.657	63.674
4+	64.466	64.467	64.4655(20)	64.466	64.471	64.465	64.463		64.473
5+	64.816	64.816		64.815	64.818	64.815			64.819
6+	64.999			64.999	65.001	64.999			
3−		62.7580(2)	62.7610(20)	62.7589	62.759	62.7588	62.758	62.7611	62.764
4−		64.1353(2)	64.1358(20)	64.1361	64.140	64.135	64.136	64.1377	64.129
5−		64.6574(2)	64.6586(20)	64.6567	64.660	64.657	64.657	64.6598	64.654
6−		64.9123(2)		64.9123		64.912	64.913		
$3d$		64.1189(2)		64.1208	64.125	64.1187	64.119	64.1217	64.158
$4d$		64.6485(4)		64.6487	64.652	64.6487	64.647	64.6485	64.667
$5d$		64.9071(5)		64.9072		64.9071	64.907		
				Width Γ (eV)					
2+	3.8[−2]	3.7[−2]	3.76(2)[−2]	3.77[−2]	4.03[−2]	3.74[−2]	3.73[−2]	3.78[−2]	3.80[−2]
3+	8.3[−3]	1.0[−2]	8.3(5)[−3]	8.26[−3]	8.96[−3]	8.19[−3]	8.32[−3]	8.27[−3]	7.64[−3]
4+	3.8[−3]	4.0(5)[−3]	3.4(7)[−3]	3.52[−3]	3.84[−3]	3.51[−3]	3.48[−3]	3.01[−3]	3.26[−3]
5+	1.4[−3]	2.0(3)[−3]		1.81[−3]	1.97[−3]	1.75[−3]		1.82[−3]	1.66[−3]
6+	8[−4]			1.04[−3]	1.04[−3]	9.8[−4]			
3−		5(3)[−4]	1.1(2)[−4]	1.05[−4]	1.13[−4]	1.05[−4]	1.16[−4]	1.06[−4]	1.42[−4]
4−		3(2)[−4]	6(2)[−5]	5.39[−5]	6.84[−5]	5.57[−5]	5.21[−5]	5.44[−5]	4.67[−5]
5−		<1[−4]	3(3)[−5]	2.53[−5]	3.34[−5]			2.65[−5]	2.00[−5]
6−				1.30[−5]					
$3d$		<5[−5]		1.1[−6]	3.30[−6]	4.4[−7]	4.41[−6]	3.3[−6]	9.00[−6]
$4d$				1.1[−7]	9.67[−7]			9.7[−7]	4.76[−6]
				Line-shape parameters q					
2+		−2.75	−2.73(4)	−2.82	−2.63				−2.81
3+		−2.5	−2.53(4)	−2.64	−2.43				−2.51
4+		−2.4	−2.58(5)	−2.59	−2.41				−2.45
5+		−2.4		−2.59	−2.40				−2.55
6+				−2.58	−2.39				
3−		−3.5	−4.1(4)	−4.83	−4.00				−4.68
4−		−3.2	−2.4(5)	−2.93	−2.32				−5.23
5−		−3.2	−2.8(5)	−3.16	−2.28				−5.75
6−				−3.19					
3d		−23		−13	−4.00				−1.07
4d		−132		−29	−12.91				−1.09

as a result of the mixture of target states $2s$ and $2p$ of He^+; while for $(sp,2n^+)$ states, the scattered electron will face the negative end of the electric dipole. For the $(2p3d)$ state, the resonance energy changes little, while the line shape changes drastically after taking into account the long-range static polarization potentials. This is an interesting question, and worthy of further theoretical study.

In order to compare with experimental and other theoretical results quantitatively, in Table IV we present the Fano parameters of the three Rydberg series of $^1P^o$ resonance.

Our Fano parameters are extracted by fitting our calculated resonance profiles to the Fano formula [2,3]. The early R-matrix calculation by Fernley, Taylor, and Seaton [21], as shown in the last column of Table IV, gave an incorrect level ordering of the $(2pnd)$ states with respect to the $(sp,2(n+1)^-)$ states. This may have resulted from the fact that the target functions they used [21] did not sufficiently take into account dynamic polarizations which influence the convergence of the calculated results. Therefore, in order to obtain the correct results, one should choose target functions carefully, and take into account sufficiently the long-range multipole potentials. As shown in Table IV, our resonance energies for all states, the widths Γ, and the q parameters for $(sp,2n^{\pm})$ states are in agreement with the experimental results and with other theoretical results. For the $(sp,2^+)$ state, our resonance energy (60.160 eV) is higher than the experimental value. This is consistent with the variational principle, and suggests that our results are not completely converged. Our result agrees with the experimental results better than the early R-matrix result [21] and the close-coupling result [19], since we have taken polarization effects sufficiently into account. Very interestingly, the doubly excited resonance structures in the He photoionization from $1s2s^{1,3}S$ metastable states are reported to have a similar accuracy [46].

Finally we would like to conclude by making some comments on the extremely narrow resonances $(2pnd)$. For the $(2pnd)$ series, the widths Γ and the q parameters calculated by various theoretical methods are quite different quantita tively. Since there exist well-resolved experiment results [7,9] for $(2p3d)$ and $(sp,24^-)$ resonance states, and the calculated results for the $(sp,24^-)$ state are in general agreement with each other, we here compare the resonance strength of the $(2p3d)$ state relative to that of the $(sp,24^-)$ state. Figure 3(a) displays our calculated spectra, which have been convoluted with the experimental resolution 4 meV; the corresponding experimental results [7] and Tang, Watanabe, and Matsuzawa's theoretical results [16] are shown in Figs. 3(b) and 3(c), respectively. The ratio of the experimental

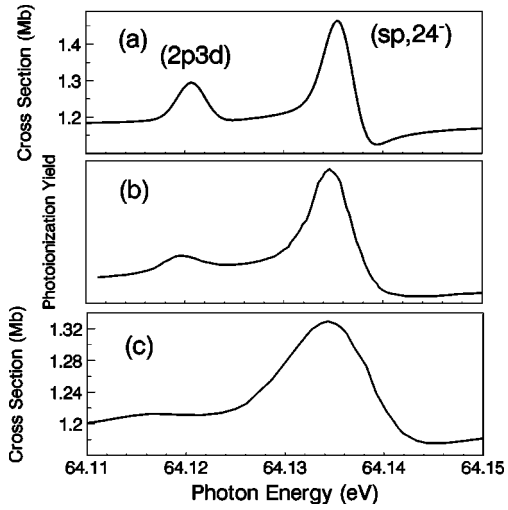

FIG. 3. The convoluted photoionization spectrum (4 meV) for $(2p3d)$ and $(sp,24^-)$ resonance states. (a) Present work. (b) The experimental result [7]. (c) Tang, Watanabe, and Matsuzawa's results [16].

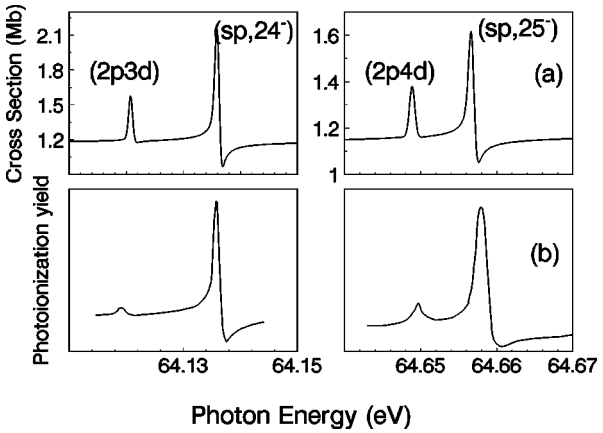

FIG. 4. The convoluted photoionization spectrum (1 meV) for $(2p3d)$, $(sp,24^-)$, $(2p4d)$, and $(sp,25^-)$ resonance states. (a) Present work. (b) The experimental result [9].

resonance strengths for the $(2p3d)$ and $(sp,24^-)$ states is about 0.25; ours is about 0.4, while that of Ref. [12] is about 0.75, and that of Ref. [16] is less than 0.1. Our theoretical results seem to be in better agreement with the experimental results. In Fig. 4, we also compare our results with the latest high-resolution measurement (1 meV) [9]. Figure 4(a) displays our calculated spectra (convoluted with 1 meV) for $(2p3d)$,$(sp,24^-)$ and $(2p4d)$,$(sp,25^-)$ pairs. The corresponding experimental results are shown in Fig. 4(b). When the resolution is improved, the resonance peaks of $(sp,2(n+1)^-)$ states increase faster than the corresponding peaks of $(2pnd)$ states. Therefore, the ratio of our calculated resonance peaks of $(2p3d)$ to $(sp,24^-)$ and $(2p4d)$ to $(sp,24^-)$ are 0.27 and 0.49, to be compared with the experimental ratios 0.10 and 0.23, respectively. The calculated strengths of $(2p4d)$ resonances are systematically larger. This is consistent with our present calculations which are not completely converged.

ACKNOWLEDGMENTS

This work was partially supported by the Chinese Science and Technology Commission, National High-Tech ICF Committee in China, Science and Technology Funds of CAEP, the Chinese Research Association for Atomic and Molecular Data, and the Chinese NSF.

APPENDIX: EIGENCHANNEL TREATMENT OF R-MATRIX THEORY

As the R-matrix code [35–37] is very powerful in calculating electron-atom collisions and photoabsorption processes (bound-bound, bound-free), and the multichannel quantum defect theory [47–55] is very powerful in analyzing atomic and molecular processes, here we combine the eigenchannel theory and R-matrix theory together, with twofold merits: (1) an analytical unified treatment of perturbed discrete Rydberg states, and autoionizing states, and their adjacent continuum to avoid numerical calculations outside the R-matrix box; and (2) a clear assignment of overlapped resonances.

Based on the R-matrix theory, the logarithmic derivative boundary matrix $\mathcal{R}(E)$ can be obtained by solving $(N+1)$-electron problem variationally within the R-matrix box with a logarithmic derivative boundary parameter b for excited electron orbitals [36]. With the $\mathcal{R}(E)$ matrix, the reaction matrix $\mathcal{K}(E)$ can be calculated with the following standing-wave expressions on the R-matrix box surface (i.e., $r=r_o$),

$$\Psi_i(E)=\mathcal{A}\Big\{\Phi_i f_i(r_o,E)-\sum_{j\leqslant N_{ph}}\mathcal{K}_{ij}\Phi_j g_j(r_o,E) - \sum_{j>N_{ph}}\mathcal{K}_{ij}\Phi_j\Theta_j(r_o)\Big\},\quad i\leqslant N_{\rm ph},$$
$$=-\mathcal{A}\Big\{\sum_{j\leqslant N_{ph}}\mathcal{K}_{ij}\Phi_j g_j(r_o,E) + \sum_{j>N_{\rm ph}}\mathcal{K}_{ij}\Phi_j\Theta_j(r_o)\Big\},\quad i>N_{\rm ph}, \tag{A1}$$

where $\mathcal{A}$ is an antisymmetrization operator. The indexes i and j denote ionization channels which are various combinations of the N-electron target states and the excited electron orbitals with the appropriate angular momentum couplings. The wave function Φ_i consists of the N-electron target-state wave function combined with the angular and spin parts of the excited electron wave function in the ith ionization channel. In a specific energy range, there are only finite channels which are responsible for spectral structures, and are called physical ionization channels ($i\leqslant N_{\rm ph}$). In the ith physical ionization channel, $f_i(r,E)$ and $g_i(r,E)$ are regular and irregular Coulombic wave functions, respectively which are continuous functions of the orbital energy across the ionization threshold, i.e., from negative to positive regions [53–55]. For the rest of the ionization channels ($i>N_{\rm ph}$), the excited electron orbitals have deeply negative orbital energies, and have exponentially decaying radial wave functions $\Theta_i(r)$ which should be negligible on the R-matrix box surface. The diagonal representation of the $N_{\rm ph}\times N_{\rm ph}$ submatrix of the reaction matrix $\mathcal{K}(E)$ defines the eigenchannels α, i.e., the eigenvalues $\tan(\pi\mu_\alpha)$ and the eigenvectors $U_{i\alpha}$ corresponding to the eigen quantum defects μ_α and orthogonal transformation matrix $U_{i\alpha}$ in MQDT. As $r\geqslant r_o$, the $N_{\rm ph}$ eigenchannel wave functions are expressed as

$$\Psi_\alpha(E)=\mathcal{A}\Big\{\sum_i \Phi_i U_{i\alpha}[f_i(r,E)\cos(\pi\mu_\alpha) - g_i(r,E)\sin(\pi\mu_\alpha)]\Big\}. \tag{A2}$$

For the case of $^1P^o$ double-excitation resonances of He around the $N=2$ threshold of He^+, our calculation involves 16 channels according to target 2. In the energy range of interest, there are only four physical ionization channels, i.e., one open physical ionization channel ($i\in P, N_p=1$) $(1s)\in p$, and three closed physical ionization channels ($i\in Q, N_q=3$)$(2s)\in p$, $(2p)\in s$, and $(2p)\in d$. Figures 5(a) and 5(b) displays the four eigenquantum defects μ_α and the six Euler angles of the 4×4 orthogonal transformation

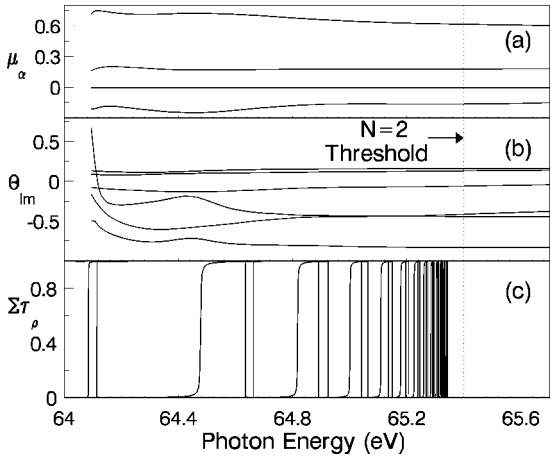

FIG. 5. Eigen quantum defects μ_α and Euler angles θ_{lm} for the $U_{i\alpha}$ matrix, and the sum of the collisional eigen phase shift $\Sigma\tau_\rho$ for He in $^1P^o$ symmetry around the $N=2$ threshold of He^+.

matrix $U_{i\alpha}$ which vary smoothly with energy. According to asymptotic boundary conditions in autoionization spectra [54,56],

$$\Psi_\rho(E)=\sum_\alpha \Psi_\alpha(E)A_\alpha^\rho \overset{r\to\infty}{\to} \mathcal{A}\Big\{\sum_{i\in P}\Phi_i T_{i\rho}\sqrt{\frac{2}{\pi k_i}} \times\sin[k_i r+qk_i^{-1}\ln(2k_i r)-l\pi/2+\sigma_i+\pi\tau_\rho] - \sum_{i\in Q}\Phi_i T_{i\rho}v_i(\nu_i,r)\Big\}, \tag{A3}$$

with $E=I_i+k_i^2/2$ as $i\in P, E=I_i-q^2\nu_i^{-2}/2$ as $i\in Q$, the ionization threshold I_i for the ith channel, the net charge q outside the R-matrix box, the Coulomb phase shift σ_i, the collisional eigen phase shift $\pi\tau_\rho$, and exponentially decaying Coulombic wave functions $v_i(\nu_i,r)$. This will lead to the following linear equations for A_α^ρ:

$$\sum_\alpha U_{i\alpha}\sin[\pi(-\tau_\rho+\mu_\alpha)]A_\alpha^\rho=0,\quad i\in P, \qquad \sum_\alpha U_{i\alpha}\sin[\pi(\nu_i+\mu_\alpha)]A_\alpha^\rho=0,\quad i\in Q. \tag{A4}$$

The nontrivial solutions of A_α^ρ leads to an equation for τ_ρ,

$$\mathrm{Det}\big|U_{i\alpha}\sin[\pi(x_i+\mu_\alpha)]\big|=0, \tag{A5}$$

with $x_i=-\tau_\rho$ as $i\in P$ and $x_i=\nu_i$ as $i\in Q$. There are N_P roots of τ_ρ ($\rho=1,2,\ldots,N_P$) and the corresponding N_P sets of A_α^ρ. Thus $T_{i\rho}$ are

$$T_{i\rho}=\sum_\alpha U_{i\alpha}\cos[\pi(-\tau_\rho+\mu_\alpha)]A_\alpha^\rho/\mathcal{N}_\rho,\quad i\in P, \qquad T_{i\rho}=\sum_\alpha U_{i\alpha}\cos[\pi(\nu_i+\mu_\alpha)]A_\alpha^\rho/\mathcal{N}_\rho,\quad i\in Q, \tag{A6}$$

with

$$\mathcal{N}_\rho^2 = \sum_{i \in P} \left\{ \sum_\alpha U_{i\alpha} \cos[\pi(-\tau_\rho + \mu_\alpha)] \right\}^2 . \qquad \text{(A7)}$$

In Fig. 5(c), we display the variation of the sum of the collisional eigenphase shifts $\Sigma_\rho \tau_\rho$, with energy which shows three series. Based on collisional eigen phase shifts τ_ρ and the mixing coefficients $T_{i\rho}$, we can trace out all resonances semianalytically, and make a definite assignment for all resonances, as shown in Table IV.

[1] R. P. Madden and K. Codling, Phys. Rev. Lett. **10**, 518 (1963); Astrophys. J. **141**, 364 (1965).
[2] U. Fano, Phys. Rev. **124**, 1866 (1961).
[3] J. W. Copper, U. Fano, and F. Prats, Phys. Rev. Lett. **10**, 518 (1963).
[4] U. Fano and J. W. Copper, Phys. Rev. **137**, A1364 (1965).
[5] M. O. Krause and F. Wuilleumier, Phys. Rev. **5**, L143 (1972); P. R. Woodruff and J. A. R. Samson, Phys. Rev. A **25**, 848 (1982); D. W. Lindle *et al.*, *ibid.* **31**, 714 (1985); H. Kossmann, B. Krassig, and V. Schmidt, J. Phys. B **21**, 1489 (1988); M. Domke, *et al.*, Phys. Rev. Lett. **66**, 1306 (1991).
[6] H. D. Morgan and D. L. Ederer, Phys. Rev. A **29**, 1901 (1984).
[7] M. Domke, G. Remmers, and G. Kaindl, Phys. Rev. Lett. **69**, 1171 (1992).
[8] M. Domke, K. Schulz, G. Remmers, and G. Kaindl, Phys. Rev. A **53**, 1424 (1996).
[9] K. Schulz, G. Kaindl, M. Domke, J. D. Bozek, P. A. Heimann, A. S. Schlachter, and J. M. Rost, Phys. Rev. Lett. **77**, 3086 (1996).
[10] D. R. Herrick and O. Sinanoglu, Phys. Rev. A **11**, 97 (1975).
[11] R. Moccia and P. Spizzo, J. Phys. B **20**, 1423 (1987).
[12] T. N. Chang, Phys. Rev. A **47**, 3441 (1993); **47**, 705 (1993).
[13] C. Froese Fischer and M. Idrees, J. Phys. B **23**, 679 (1990).
[14] J. Macek, J. Phys. B **1**, 831 (1968).
[15] C. D. Lin, Phys. Rev. A **10**, 1986 (1974); **25**, 76 (1982).
[16] J. Z. Tang, S. Watanabe, and M. Matsuzawa, Phys. Rev. A **48**, 841 (1993); **46**, 2437 (1992).
[17] P. G. Burke and D. D. McVicar, Proc. Phys. Soc. London **86**, 989 (1965).
[18] D. H. Oza, Phys. Rev. A **33**, 824 (1986).
[19] S. Salomonson, S. L. Carter, and H. P. Kelly, Phys. Rev. A **39**, 5111 (1989).
[20] K. A. Berrington, P. G. Burke, W. C. Fon, and K. T. Taylor, J. Phys. B **15**, L603 (1982).
[21] J. A. Fernley, K. T. Taylor, and M. J. Seaton, J. Phys. B **20**, 6457 (1987).
[22] P. Hamacher and J. Hinze, J. Phys. B **22**, 3397 (1989).
[23] R. Gersbacher and J. T. Broad, J. Phys. B **23**, 365 (1990).
[24] K. T. Chung and I-hsiun Chen, Phys. Rev. Lett. **28**, 783 (1972).
[25] K. T. Chung and B. F. Davis, Phys. Rev. A **22**, 835 (1980); **26**, 3278 (1982); **31**, 1187 (1985).
[26] A. K. Bhatia and A. Temkin, Phys. Rev. A **29**, 1895 (1984).
[27] A. Macias, F. Martin, A. Riera, and M. Yanez, Phys. Rev. A **36**, 4187 (1987).
[28] J. M. Seminario and F. C. Sanders, Phys. Rev. A **42**, 2562 (1990).
[29] I. Sanchez and F. Martin, J. Phys. B **23**, 4263 (1990).
[30] L. Wu and J. Xi, J. Phys. B **23**, 727 (1990).
[31] Y. K. Ho, Phys. Rev. A **23**, 2137 (1981).
[32] Y. K. Ho, Z. Phys. D **21**, 191 (1991).
[33] U. Fano, Rep. Prog. Phys. **46**, 97 (1983).
[34] P. G. Burke, A. Hibbert, and W. D. Robb, J. Phys. B **4**, 153 (1971).
[35] K. A. Berrington, P. G. Burke, J. J. Chang, A. T. Chivers, W. D. Robb, and K. T. Taylor, Comput. Phys. Commun. **8**, 149 (1974).
[36] K. A. Berrington, P. G. Burke, M. Le Dourneuf, W. D. Robb, K. T. Taylor, and Lan Vo Ky, Comput. Phys. Commun. **14**, 346 (1978).
[37] K. A. Berrington, P. G. Burke, K. Butler, M. J. Seaton, P. J. Storey, K. T. Taylor, and Yan Yu, J. Phys. B **20**, 6379 (1987).
[38] L. VoKy, H. E. Saraph, W. Eissner, Z. W. Liu, and H. P. Kelly, Phys. Rev. A **46**, 3945 (1992).
[39] Jia-Ming Li, L. VoKy, Yi-Zhi Qu, J. Yan, Pei-Hong Zhang, H. S. Zhou, and P. Faucher, Phys. Rev. A **55**, 3239 (1997).
[40] Jia-Ming Li, L. VoKy, J. Yan, and Yi-Zhi Qu, Chin. Phys. Lett. **13**, 902 (1996).
[41] G. Herzberg, Proc. R. Soc. London, Ser. A **248**, 309 (1958).
[42] *Atomic Energy Levels*, edited by C. E. Moore, Natl. Bur. Stand. Natl. Stand. Ref. Data Ser. No. 35 (U.S. GPO, Washington, D.C., 1971), Vol. I.
[43] M. Le Dourneuf (unpublished); Vo Ky Lan, M. Le Dourneuf, and P. G. Burke, J. Phys. B **9**, 1065 (1976); J. F. Thornbury and A. Hibbert, *ibid.* **20**, 6447 (1987).
[44] C. L. Pekeris, Phys. Rev. **126**, 1470 (1962).
[45] J. McI. Calvert and W. D. Davison, J. Phys. B **4**, 314 (1971).
[46] T. K. Fang and T. N. Chang, Phys. Rev. A **56**, 1650 (1997).
[47] M. J. Seaton, Proc. Phys. Soc. London **88**, 801 (1966).
[48] U. Fano, Phys. Rev. A **2**, 353 (1970).
[49] C. M. Lee (Jia-Ming Li), Phys. Rev. A **10**, 584 (1974).
[50] U. Fano, J. Opt. Soc. Am. **65**, 979 (1975).
[51] C. Greene, U. Fano, and G. Strinati, Phys. Rev. A **19**, 1485 (1979).
[52] C. M. Lee (Jia-Ming Li) and W. R. Johnson, Phys. Rev. A **22**, 979 (1980).
[53] Jia-Ming Li, Acta Phys. Sin. **29**, 419 (1980).
[54] Jia-Ming Li, Acta Phys. Sin. **32**, 84 (1983).
[55] M. J. Seaton, Rep. Prog. Phys. **46**, 167 (1983).
[56] C. M. Lee (Jia-Ming Li), Phys. Rev. A **10**, 1598 (1974).